Guided ultrasonic wave monitoring techniques to assess bone implant loosening

Enze Chen, Krishnan Balasubramaniam, Prabhu Rajagopal, Paul Fromme

Enze Chen, Krishnan Balasubramaniam, Prabhu Rajagopal, Paul Fromme, "Guided ultrasonic wave monitoring techniques to assess bone implant loosening," Proc. SPIE 12488, Health Monitoring of Structural and Biological Systems XVII, 1248825 (25 April 2023); doi: 10.1117/12.2659366

SPIE.

Event: SPIE Smart Structures + Nondestructive Evaluation, 2023, Long Beach, California, United States

Guided ultrasonic wave monitoring techniques to assess bone implant loosening

Enze Chen[a], Krishnan Balasubramaniam[b], Prabhu Rajagopal[b], Paul Fromme[a]
[a]Department of Mechanical Engineering, University College London, WC1E 7JE, UK
[b]Center for Nondestructive Evaluation, IIT Madras, Chennai 600036, INDIA

ABSTRACT

Total ankle replacement (TAR) is the main clinical treatment for end-stage ankle arthritis, replacing the ankle joint with a metallic implant. Component loosening, fracture, and wear are the main reasons for implant failure, requiring revision surgery. A non-invasive guided wave monitoring technique is being developed to ultimately evaluate in-vivo implant device integrity and bone-implant interface conditions (osseointegration). Finite Element (FE) simulations were performed to investigate the feasibility and sensitivity of ultrasonic monitoring of the interface conditions, assessing suitable guided wave modes and excitation frequencies. A simplified implant geometry was developed for FE modelling in Abaqus/Explicit. Selected guided wave modes (higher-order longitudinal modes sensitive to bone/implant interface changes) were excited at the distal end of the metallic implant component for detection of variations of bone-implant contact conditions. Simulation results showed the feasibility for guided ultrasonic waves to monitor bone implant osseointegration. Guided wave signal amplitude and changes of arrival time of pulses propagating along the metallic implant can indicate the presence of improved osseointegration. The potential for the integration of the bone implant monitoring sensors and other biosensors into secure, blockchain-based, remote patient data management systems will be further investigated.

Keywords: Finite Element Modelling, Guided Wave Monitoring, Osseointegration, Total Ankle Arthroplasty, Blockchain

1. INTRODUCTION

Total ankle replacement (TAR) provides instant pain relief and restores ankle motion for patients, replacing the ankle joint with a prosthetic component consisting of two metal components and a polyethylene liner. Implant loosening and polyethylene liner wear are the two major problems leading to TAR implant failure [1]. The average intake age in the UK for female and male patients are 66 and 68 years, respectively. Nearly 4000 ankle replacement procedures have been recorded from 2010 to 2017 in the UK. The number of replacement procedures has grown rapidly, especially in the last two years of the record, with 726 replacement cases in 2015 and 839 cases in 2016 [2]. Ankle arthrodesis (AA) is the alternative for the surgical management of ankle arthritis. It is commonly used after revision surgery due to TAR implant failure or used for patients with poor physical condition. After resecting the articular cartilage surface of the talus and tibia joint, the proximal epiphysis of the talus and distal epiphysis of the tibia are fused together. Total ankle arthrodesis provides instant paint relief and decreases surgical time and risk of revision for patients compared to TAR. Vakhshori et al. [3] compared patients undergoing AA and TAR from 2007 to 2013 and found similar American Orthopaedic Foot and Ankle Society ankle-hindfoot scores, indicating that the treatment outcomes are comparable. However, AA altered the gait mechanics and velocity, and decreased the range of motion, which may result in osteoarthritis on the adjacent joints, while TAR improved the range of motion with less load on surrounding joints and improved gait. The suitable intake patient for ankle joint replacement needs to satisfy the following criteria: good bone stock, excellent hind foot-ankle alignment, and normal vascular status [4].

Implant loosening after TAR is the most common issue for both tibia and talus at 18% [1]. Bone remodeling and mass loss, stress shielding, and implant-bone interface conditions may contribute to loosening and subsidence of the tibial and talar component [5]. Bone remodeling may cause excessive bone resorption around the implant, resulting in implant loosening. Stress shielding is caused by the difference in stiffness between implant and bone tissue and the change of loading conditions [6]. It decreases the typical stress levels in normal bone tissue and can eventually lead to bone density reduction and bone resorption that can cause implant loosening. Wear of the polyethylene liner can result in loosening or

Health Monitoring of Structural and Biological Systems XVII, edited by
Paul Fromme, Zhongqing Su, Proc. of SPIE Vol. 12488, 1248825
© 2023 SPIE · 0277-786X · doi: 10.1117/12.2659366

mechanical damage of the liner, leading to potential dislocation of the ankle prosthetic. The shear and torsion loading conditions of the TAR implant polyethylene liner impacts the level of wear. The loading condition typically include compressive load applied to the proximal end of the tibia and fibula, uniform pressure on the talar component, or static loading for the talar component [7].

The condition of the implant fixation is crucial for the stability of orthopedic implants, which include hip, knee, and ankle implants. Dahl et al. [8] used a Doppler ultrasound technique to detect the osseointegration of the Agility implant. An electromagnetic actuator excited vibrations in cadaveric ankles samples and the resonant wave was received by a linear-array ultrasound transducer. Wang and Lynch [9] studied the use of longitudinal guided wave modes to monitor the loosening of femoral implants. They developed a finite element (FE) model for an osseointegrated implant to investigate the relationship of the energy of the fundamental longitudinal wave mode with the osseointegration at the bone-implant interface. A similar model was used [10] to identify the location of cracks in the bone by analyzing reflected Rayleigh waves. The differences of the waveform in the time-amplitude domain can indicate bone cracks, and the arrival time of the Rayleigh waves can determine the location of the defect.

Guided wave monitoring techniques are being developed to monitor TAR implant integrity using a Structural Health Monitoring (SHM) approach. Guided waves can propagate long distances with minimal attenuation along thin structures, with wave signal changes indicating the position of defects and damage. Longitudinal, torsional, and flexural guided wave could potentially be employed to measure the healing of long bones [11]. Ultrasonic waves were found to show only limited variation to the assumed material anisotropy (orthotropic, quasi-isotropic) for bone plate model testing [12]. Simplified geometry (hollow cylinders models) with a semi-analytical setup could be used for guided wave testing and compared with experiments using sawbones [13] to evaluate the feasibility of the guided wave excitation technique. Osseointegration was examined by the comparison of incident and reflected waves from the changing bone-implant interface. Absorbing layers using increasing damping (ALID) [14] could potentially be applied to suppress wave reflections at the proximal end of the modelled bone to correlate better with the actual bone geometry. A periodic excitation (comb) approach can be applied [15] to enhance the excitation of the dominant mode in the longitudinal direction. Remote monitoring of patient recovery and home healthcare must overcome challenges in properly indexing the data collected from different sensors, and in storing and retrieving information securely. Work has been conducted on a blockchain-based approach for the management of health records [16], which permits indexing patient-centric information using unique and immutable tags that can then be tracked securely across geographies and organizations.

In this contribution a guided wave monitoring technique is being developed to monitor potential component loosening and the osseointegration process to ensure in-vivo implant integrity. A simplified cylindrical FE model for a femoral amputee was developed in ABAQUS/Explicit for evaluating the suitability and sensitivity of longitudinal guided wave mode propagation in the bone implant. In the next section, the FE model and guided wave simulation are described. Section 3 explains the selection of a suitable guided wave mode, while section 4 evaluates the predicted wave propagation in the implant and bone-implant interface for different stages of osseointegration and the sensitivity for monitoring of changes. Finally, section 5 discusses the integration of the guided wave-based sensor data into a blockchain-based framework for the management of patient records and sensor logs.

2. FINITE ELEMENT SIMULATIONS

Finite element simulations using the commercial software Abaqus were employed to investigate suitable guided wave modes and to predict the sensitivity to bone-implant interface changes. To simulate the implant and attached limb, three simplified parts were generated in the model as shown in Fig. 1. The inner Ti-6AL-4V implant is modelled as a 14 mm diameter cylinder with Young's modulus of 110 GPa, density of 4429 kg/m^3, and Poisson's ratio of 0.3. The bone-implant interface layer is modelled as a thin hollow cylinder of 1 mm thickness. To simulate the changes in osseointegration, the material property of the bone-implant interface was changed from very soft tissue (Young's modulus 1 kPa, density 1 kg/m^3) to cortical bone (Young's modulus 20 GPa, density 942 kg/m^3), with a fixed Poisson's ratio of 0.38. The outer layer femoral bone is modelled as a hollow cylinder (inner diameter 16 mm, outer diameter 26 mm) with the properties of cortical bone (see Fig. 1). A simplified cylindrical model was chosen as a reasonable representation of the femoral anatomy. Cylindrical models were shown to have similar stress states compared with a FE model of the bone anatomy and implant for torsional, axial, and bending loads [17]. The material properties of the models were set to be isotropic with low Rayleigh damping (β = 1 ns). Though cortical bone is an orthotropic material, an isotropic model was employed as stress and displacement are mainly investigated in the longitudinal direction with axial loading (compressional wave).

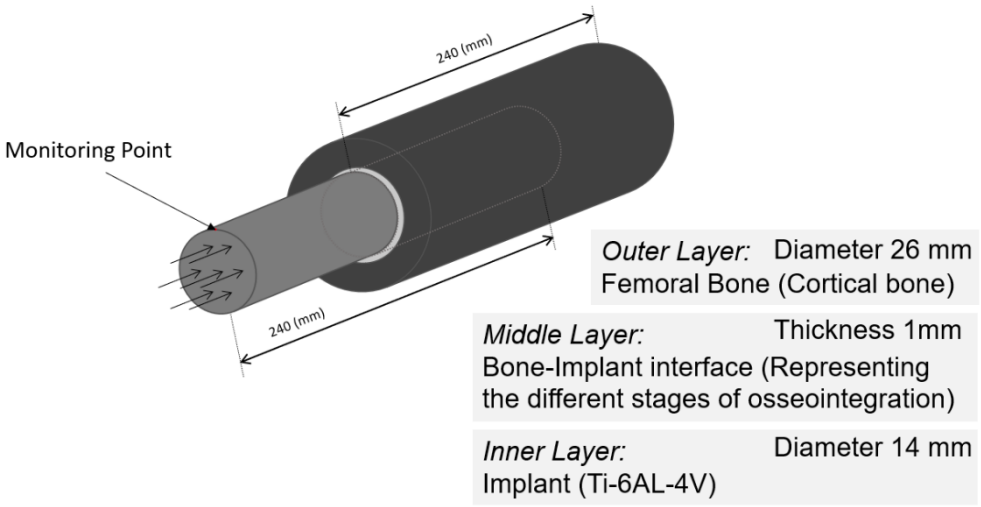

Figure 1. Schematic of cylindrical bone implant model and guided wave excitation.

Linear hexahedral elements (C3D8R) were chosen for the bone and soft tissue with 1 mm global element size for the mesh of the bone part (81'704 elements) and 0.2 mm for the soft tissue part (977'955 elements), achieving a uniform mesh for the hollow cylinders. The global element size is 0.2 mm for the implant mesh with a mix of linear hexahedral elements (C3D8R, 3'744'000 elements) along the outer ring and linear wedge elements (C3D6, 124'800 elements) in the central part to obtain a more uniform mesh in the solid middle part. ABAQUS/Explicit was used to simulate the wave propagation and reflection. The time step increment was fixed as 1 ns and the total time period of the FE simulation was 18 μs. The selected element size and time step fulfill the usual stability criterion (time step smaller than propagation time across one element, element size 1/10th of minimum wavelength) to accurately simulate the wave propagation.

The selected guided wave was excited as 5 sinusoidal cycles in a Hanning window with a center frequency of 350 kHz. As shown schematically in Fig. 1, the excitation was applied at the distal end of the implant as longitudinal displacement. The amplitude of the wave displacement was varied with the radius to match the mode shape across the cylinder diameter. The axial displacement at the inner ring (1 mm radius circle) is half of the magnitude of the displacement in the outer ring (5 mm inner radius and 7 mm outer radius hollow circle) with opposite direction to match the mode shape of the selected guided wave along the implant depth. The guided wave pulse was excited at the distal end of the implant (incident wave) and the reflected wave from the proximal implant end (within the bone) was recorded at 10 monitoring points along the bone implant.

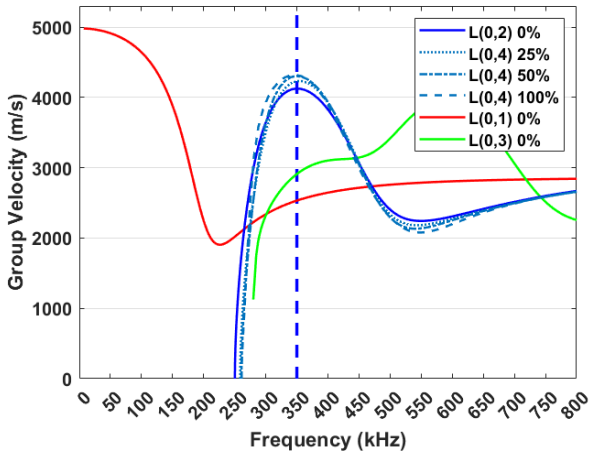

Figure 2. Dispersion diagram of longitudinal guided wave modes group velocity for implant (0% integration), with variation of L(0,4) mode for different stages of osseointegration at bone-implant interface.

3. GUIDED WAVE MODE SELECTION

Different guided wave modes and excitation frequencies were assessed for their suitability to monitor changes of the bone-implant interface (osseointegration – modelled as changes of the interface layer property). The ideal guided wave mode should uniformly propagate along both the implant and implant-bone structure with minimal dispersion and be sensitive to osseointegration changes. Dispersion diagrams were obtained using the Disperse software. Figure 2 shows the group velocity dispersion curves for the lower order longitudinal modes and the selected wave mode at different stages of osseointegration in the bone-implant interface. The L(0,2) longitudinal guided wave mode in the cylindrical implant exhibits a plateau with the highest group velocity (approximately 4000 m/s) around 350 kHz excitation frequency. It converts to the L(0,4) wave mode when propagating into the bone-implant interface, but the dispersion curve retains a similar shape through the changes in osseointegration. The group velocity at 350 kHz increases slightly with increasing osseointegration.

The L(0,2) wave mode is distinguishable from the L(0,1) longitudinal guided wave mode, which has the fastest group velocity and is reasonably non-dispersive at low frequencies up to about 100 kHz, but has lower velocity at 350 kHz excitation frequency. However, the L(0,3) guided wave mode has a similar cut-off frequency as the L(0,2) wave mode and behavior (group velocity plateau) around the 350 kHz frequency region. The mode shapes for the 350 kHz L(0,2) and L(0,3) modes in the titanium implant are shown in Fig. 3(a) and exhibit some similarities. The L(0,3) mode has the closest group velocity to the L(0,2) mode at about 3000 m/s. The L(0,3) guided wave mode could be inadvertently excited alongside the incident wave L(0,2) in the implant as a secondary wave pulse.

The mode shapes (axial and radial displacement) for the respective L(0,2) mode in the implant cylinder and L(0,4) mode in the 3 layer model along the implant radius are very similar, as shown in Fig. 3(b). The 350 kHz L(0,2) wave mode can convert to the L(0,4) wave mode at the bone interface entry with limited wave reflection and thus amplitude loss since they have similar properties. The L(0,4) wave mode shows sensitivity to the bone-implant interface due to the significant axial displacement (and gradient) in the interface layer. Compared to the first longitudinal L(0,1) guided wave mode at low frequencies (below 100 kHz, where the L(0,1) mode is the first arrival and reasonably non-dispersive), the L(0,2) wave mode has a relatively short wavelength (16 mm at 350 kHz) compared to the expected 240 mm implant length, minimizing the overlap in time of multiple wave pulses and reflections. Though the wave mode nomenclature changes, the wave propagation remains mostly stable and the selected mode can propagate both along the implant and implant-bone interface. Therefore, the 350 kHz L(0,2) wave mode was chosen for further examination in the FE simulations.

4. RESULTS AND DISCUSSION

The wave propagation in the implant and bone-implant interface was investigated and predicted waveforms from the FE simulations were compared to assess the sensitivity of the selected guided wave mode for monitoring of changes. The guided wave pulse (350 kHz L(0,2) axial symmetric longitudinal wave) was excited at the distal end of the implant and the reflected wave from the proximal implant end (within the bone) received by a sensor at the distal end of the bone implant as shown in Fig. 4.

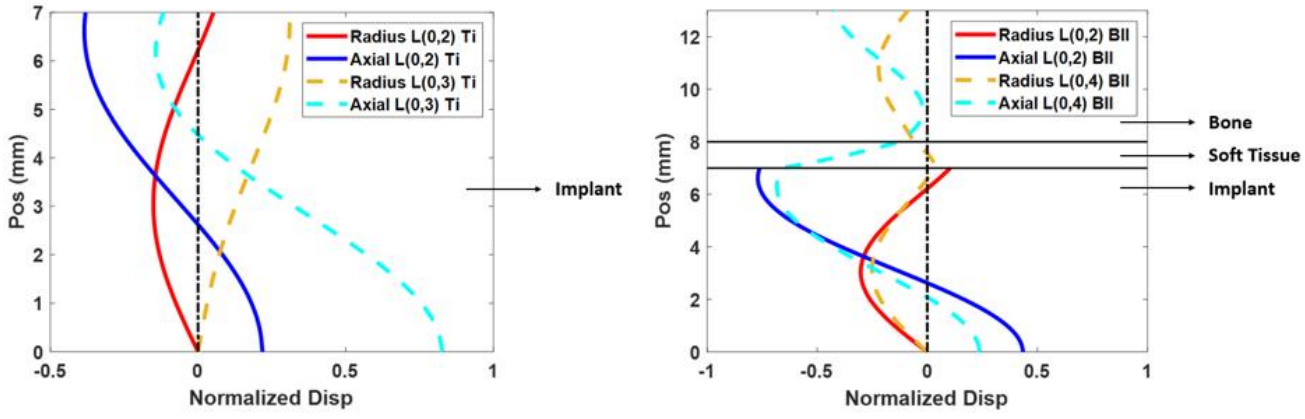

Figure 3. (a) Mode shape of L(0,2) and L(0,3) 350 kHz in titanium implant; (b) mode shape of L(0,2) 350 kHz in titanium implant and L(0,4) 350 kHz in 3 layer model with 50% osseointegration bone-implant interface.

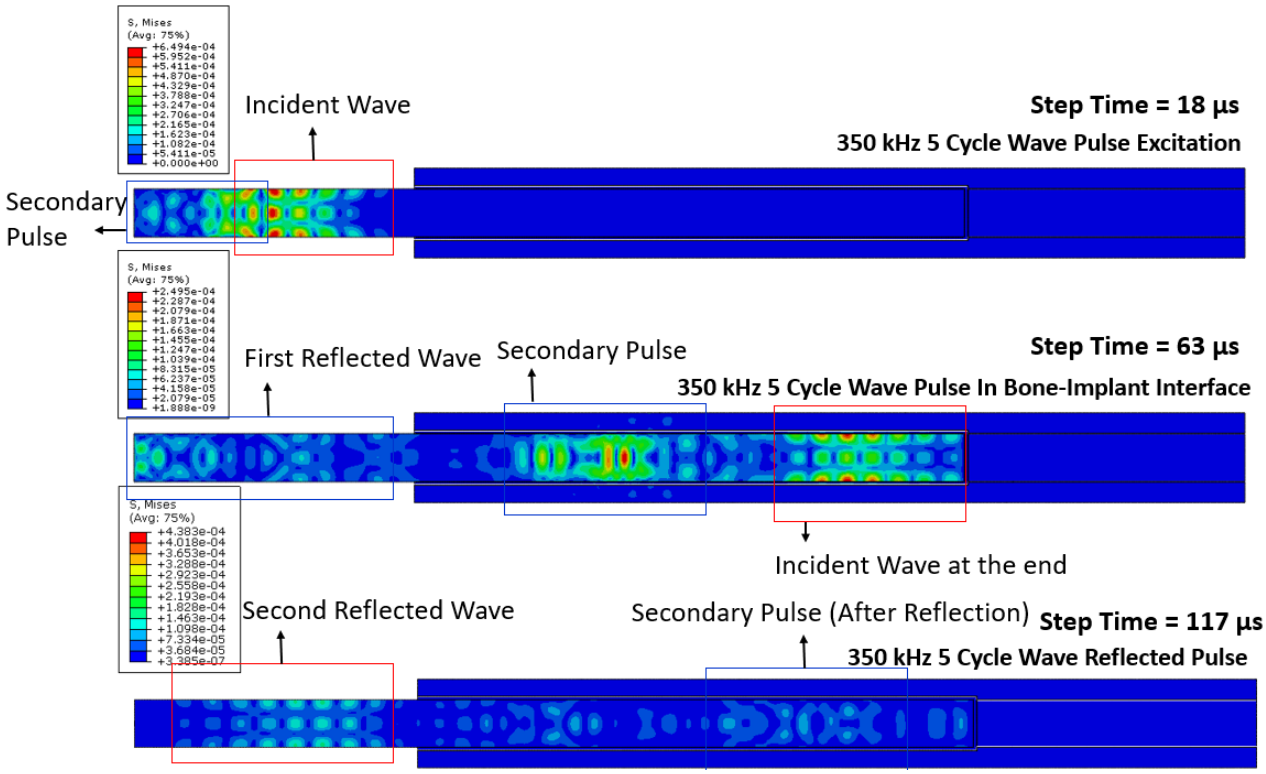

Figure 4. Contour plot of von Mises stress at different time steps for 350 kHz, 5 cycle incident L(0,2) wave mode for 50% osseointegration condition.

Figure 4(a) shows the incident wave propagation before entering the bone-implant interface, a secondary pulse is generated alongside the main incident wave. The incident wave propagation in the bone-implant interface can be observed in Fig. 4(b). When the incident wave enters the bone-implant interface, a small, reflected wave is generated, propagating in the opposite direction. However, this first reflection is difficult to detect at the distal end due to its low amplitude and the time traces (Fig. 5, 60-80 µs) show no significant wave energy changes. The main incident wave is clearly visible at the end of the metallic implant with the same wave mode across the diameter and some limited energy leakage into the bone. The secondary excited pulse is distinguishable with a lower propagation velocity. The main (second) reflected wave is generated at the proximal end of the implant as shown in Figure 4(c) and propagates back towards the distal end. The second reflected wave shows sensitivity to the osseointegration with energy loss during the propagation along the bone-implant interface. When the second reflected wave returns to the distal end of the implant, it has become the most dominant wave pulse and is predicted to be recognizable in an experimental setup.

As shown in Fig. 5, the predicted guided wave time traces recorded at the distal end of the implant contain the incident wave, secondary pulse and second reflected wave (incident wave after reflection at the proximal end of the implant). From 0-20 µs, the incident wave L(0,2) was excited, with a small secondary pulse which could be the L(0,3) wave mode as described above. From 120-140 µs, the second (main) reflected wave at the distal end of the implant can be clearly identified from the time traces. The time traces correlate well with the contour plot results shown in Fig. 4. The second reflected wave pulse loses approximately 80% energy compared to the incident wave (for 50% osseointegration) from interface reflection and energy leakage into the bone-implant interface as analyzed above, showing the sensitivity to the changes of osseointegration. Thus, despite the generation of the L(0,3) secondary pulse, excitation of the longitudinal (L0,2) guided wave at the 350 kHz provides a suitable wave mode for osseointegration detection.

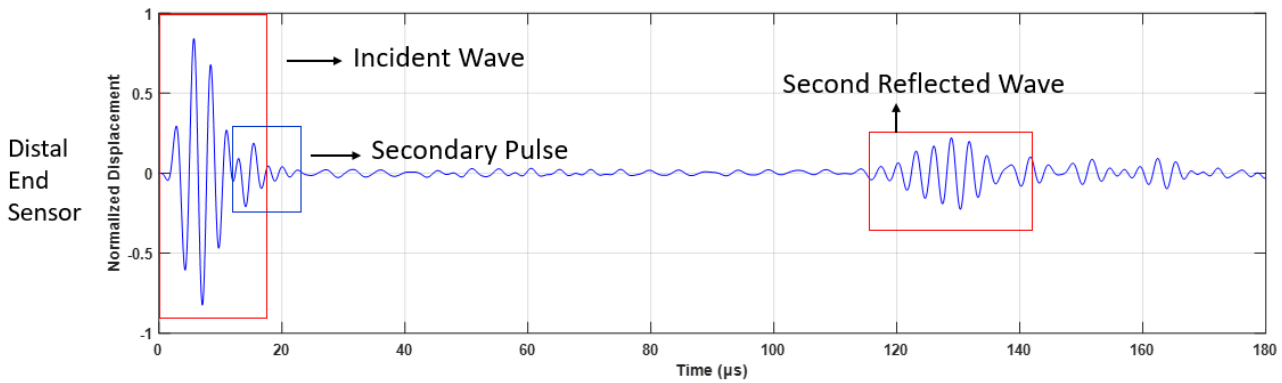

Figure 5. Time trace (normalized displacement) monitored at the distal end of the implant, 350 kHz 5 cycle incident L(0,2) wave mode for 50% osseointegration condition.

The maximum amplitude and arrival time of the envelope of the second (main) reflected wave, as shown in Fig. 6, were evaluated as initial osseointegration indicators. Different stages of osseointegration, modelled as changes in the bone-implant interface layer, influence the attenuation and group velocity of the reflected wave at the proximal end, received at the simulated sensor at the distal end around 120-140 μs in the time traces. At 0% osseointegration (very soft interface layer), the reflected wave amplitude already decreases due to dispersion. With increasing osseointegration, the maximum amplitude decreases further, and the arrival times increases. At high levels of osseointegration (50% to 100%), the exact arrival time and maxima of the wave were not easily distinguishable due to dispersion and similar wave envelopes.

Figure 7 shows the dependence of amplitude and arrival time on the increase of osseointegration. The amplitude of the reflected guided pulse is sensitive to changes at the initial stage of osseointegration up to 50%) but lacks sensitivity at the final stages of osseointegration. Improvements of the signal processing or chosen wave mode will be required to differentiate high levels of osseointegration. The arrival time changes consistently with the degree of osseointegration, but only in a small range (125-130 μs) and not fully consistent with predicted changes to the group velocity. Future investigation will be required to assess the effects of osseointegration on arrival times and the sensitivity of the reflected guided wave mode to higher level of osseointegration.

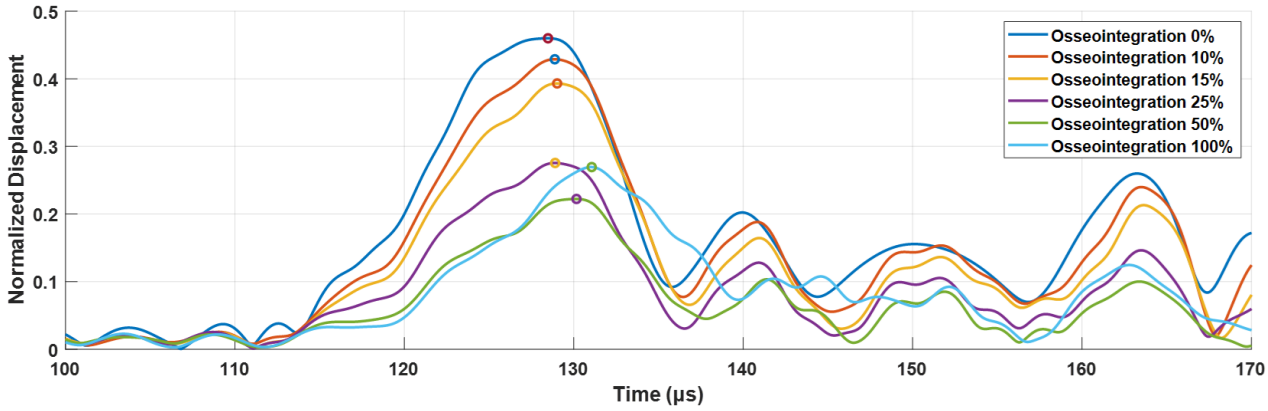

Figure 6. Envelope (absolute value of Hilbert transform) of time traces (reflected 350 kHz, 5 cycle wave pulse) at the distal end of the implant for different stages of osseointegration.

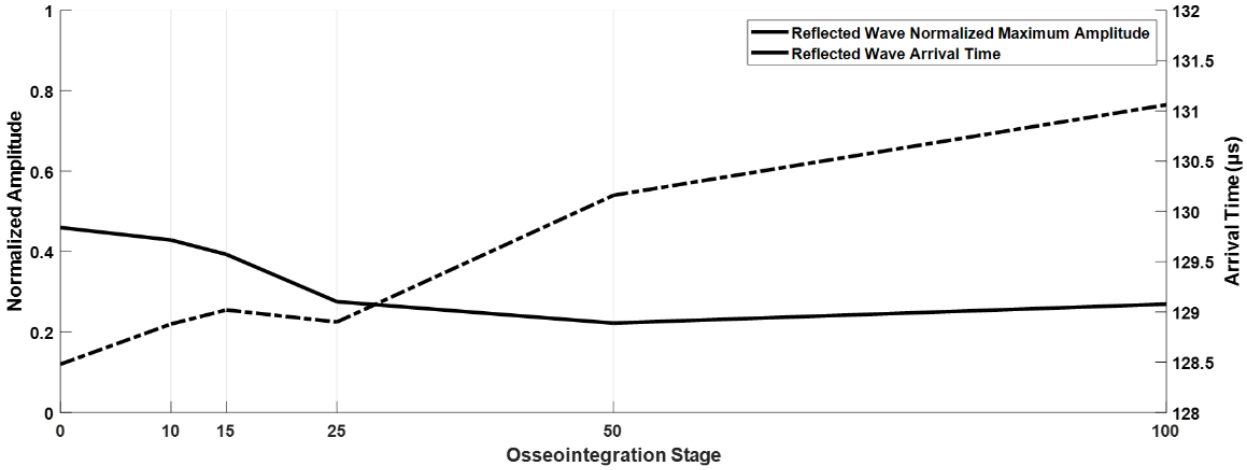

Figure 7. Maximum amplitude (reflected pulse) and arrival time changes with increase of osseointegration; L(0,2) longitudinal guided wave mode at 350 kHz.

5. BLOCKCHAIN BASED HEALTH RECORD MANAGEMENT SYSTEM

Current work includes the development of a framework for the integration of this guided wave-based system into a secure blockchain-based system for the secure management of health records. The use of blockchain helps to evolve a unique identifier for every patient, and all health records including doctor consultations, biosensor measurements, pharmacy and therapy, and interventions are hence securely connected. A relay server which acts as a 'Blockchainiser,' is being developed, which interfaces with biosensors (such as the guided wave-based bone condition monitoring system described above), as well as prescriptions and doctor recommendations. The flow of information as envisaged, integrating biosensors into the blockchain-based health record management system, is shown in Fig. 8 below. The relay server (or Blockchainiser) obtains information, and then converts this into a suitable format before pushing this to the cloud or a local chain as suitable for home or hospital situations, respectively. Currently, the blockchain team is working on time-domain data obtained from the guided wave bone condition monitoring system, and storing this into the health record management system, in the form of raw signals and PDF views. A number of functionalities will be added in a modular manner, that will be uniquely indexed to a patient, as well as permitting access and visualization operations.

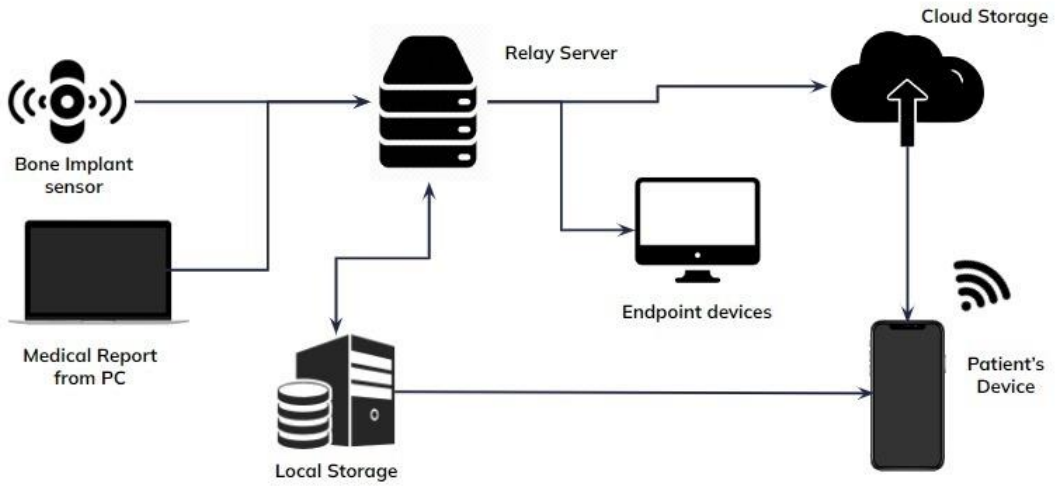

Figure 8: Flow of information as envisaged, integrating biosensors into the blockchain-based health record management system: the relay server obtains information, and converts this into a suitable format before pushing this to the cloud or a local chain as suitable for home or hospital situations, respectively.

6. CONCLUSIONS

Component loosening is one of the main factors for bone implant failure that may require revision operation. It is mainly caused by incomplete osseointegration during the bone healing process. A non-invasive ultrasonic monitoring technique was evaluated to investigate the feasibility of osseointegration detection and monitoring. The axial symmetric, longitudinal L(0,2) guided wave mode at 350 kHz was selected based on the dispersion diagrams for a simplified cylindrical model of the relevant implant and bone geometry. Using FE modelling, guided ultrasonic wave measurements of the implant-bone structure were simulated, requiring only access to the distal end of a femoral implant. The FE simulation predicted promising results for the examination of bone-implant changes, but limited sensitivity for the final stages of osseointegration. Improved excitation will be required to suppress secondary guided wave modes and the predicted sensitivity will need to be verified experimentally. The connection of this system in a seamless manner to a secure platform for the management of digital patient health records is discussed.

REFERENCES

[1] Chen, J., Akoh, C. C., Kadakia, R. et al., "Analysis of 408 Total Ankle Arthroplasty Adverse Events Reported to the US Food and Drug Administration From 2015 to 2018," Foot Ankle Spec, 14(5), 393-400 (2021).

[2] HQIP, [Public and Patient Guide to the main NJR Annual Report], (2018).

[3] Vakhshori, V., Sabour, A. F., Alluri, R. K. et al., "Patient and Practice Trends in Total Ankle Replacement and Tibiotalar Arthrodesis in the United States From 2007 to 2013," J Am Acad Orthop Surg, 27(2), e77-e84 (2019).

[4] Saltzman, C. L., Mclff, T. E., Buckwalter, J. A. et al., "Total Ankle Replacement Revisited," Journal of Orthopaedic & Sports Physical Therapy, 30(2), 56-67 (2000).

[5] Sofia, D., "Biomechanics of the Total Ankle Arthroplasty: Stress Analysis and Bone Remodeling Biomedical Engineering Examination Committee," pp.1–134 (2013).

[6] Bouguecha, A., Weigel, N., Behrens, B.-A. et al., "Numerical simulation of strain-adaptive bone remodelling in the ankle joint," BioMedical Engineering OnLine, 10(1), 1-13 (2011).

[7] Mondal, S., and Ghosh, R., "Experimental and finite element investigation of total ankle replacement: A review of literature and recommendations," J Orthop, 18, 41-49 (2020).

[8] Dahl, M. C., Kramer, P. A., Reinhall, P. G. et al., "The efficacy of using vibrometry to detect osteointegration of the Agility total ankle," J Biomech, 43(9), 1840-3 (2010).

[9] Wang, W., and Lynch, J. P., "IWSHM 2017: Application of guided wave methods to quantitatively assess healing in osseointegrated prostheses," Structural Health Monitoring, 17(6), 1377-1392 (2018).

[10] Wang, W., and Lynch, J. P., "Identification of bone fracture in osseointegrated prostheses using Rayleigh wave methods." 10600, 254-263.

[11] Protopappas, V. C., Fotiadis, D. I., and Malizos, K. N., "Guided ultrasound wave propagation in intact and healing long bones," Ultrasound Med Biol, 32(5), 693-708 (2006).

[12] Takano, K., Nagatani, Y., and Matsukawa, M., "Simulation study of axial ultrasound transmission in heterogeneous cortical bone model," Japanese Journal of Applied Physics, 56(7S1), (2017).

[13] Abid, A., Pereira, D., Fernandes, J. C. et al., "Sensitivity Study of Ultrasonic Guided Waves to Cortical Bone Mechanical Properties with Axial and Circumferential Propagation," Acta Acustica united with Acustica, 103(3), 421-429 (2017).

[14] Rajagopal, P., Drozdz, M., Skelton, E. A. et al., "On the use of absorbing layers to simulate the propagation of elastic waves in unbounded isotropic media using commercially available Finite Element packages," NDT & E International, 51, 30-40 (2012).

[15] Antony Jacob, A., Rajagopal, P., and Balasubramaniam, K., "Selective modal excitation for optimization of waveguide based bulk ultrasonic transducers," NDT & E International, 94, 47-55 (2018).

[16] Rana, A., and Rajagopal, P., [Method and blockchain device for managing health records of users in blockchain based collaborative network], patent filed with Indian Patent Office, 202141006659 (17/02/2022).

[17] Newcombe, L., Dewar, M., Blunn, G. et al., "Effect of amputation level on the stress transferred to the femur by an artificial limb directly attached to the bone," Medical Engineering & Physics, 35(12), 1744-1753 (2013).